Optimal bone mechanical and material properties require a functional glucagon-like peptide-1 receptor.

Guillaume Mabilleau, Aleksandra Mieczkowska, Nigel Irwin, Peter-R. Flatt, Daniel Chappard

Optimal bone mechanical and material properties require a functional GLP-1 receptor

Guillaume Mabilleau[1,2], Aleksandra Mieczkowska[1], Nigel Irwin[3], Peter R. Flatt[3], Daniel Chappard[1,2]

[1] : GEROM Groupe Etudes Remodelage Osseux et bioMatériaux – LHEA, and [2] Service Commun d'Imageries et d'Analyses Microscopiques (SCIAM), IRIS-IBS Institut de Biologie en Santé, LUNAM Université, CHU d'Angers, 49933 ANGERS Cedex -FRANCE.

[3]: School of Biomedical Sciences, Ulster University, Coleraine, United Kingdom

Running title: Bone strength in GLP-1R KO mice

Please send all correspondence to:

Guillaume Mabilleau, PhD
GEROM-LHEA UPRES EA 4658
Institut de Biologie en Santé
Université d'Angers
4 rue Larrey
49933 Angers Cedex 09
France

☎ : +33(0) 244 688 349
Fax : +33(0) 244 688 350
✉ : guillaume.mabilleau@univ-angers.fr

Keywords: Bone quality; Glucagon like peptide-1; bone strength, bone matrix; bone mineral.
Word count: 3751

ABSTRACT

Bone is permanently remodeled by a complex network of local, hormonal and neuronal factors that affect osteoclast and osteoblast biology. Among these factors a role for gastro-intestinal hormones has been proposed based on evidence that bone resorption dramatically falls after a meal. Glucagon like peptide-1 (GLP-1) is one of these gut hormones and despite several reports suggesting an anabolic effect of GLP-1, or its stable analogues, on bone mass, little is known about the effects of the GLP-1/GLP-1 receptor on bone strength. In the present study we investigated by three-point bending, quantitative x-ray microradiography, microCT, qBEI and FTIRI bone strength and bone quality in male GLP-1R knockout (GLP-1R KO) mice as compared with control wild-type (WT) animals. Animals with a deletion of the GLP-1R presented with a significant reduction of ultimate load, yield load, stiffness, total absorbed and post-yield energies as compared with WT animals. Furthermore, cortical thickness and bone outer diameter were significantly decreased in deficient animals. The mineral quantity and quality were not significantly different between GLP-1R KO and WT animals. On the other hand, the maturity of the collagen matrix was significantly reduced in deficient animals and associated with lowered material properties. Taken together, these data support a positive effect of the GLP-1R on bone strength and quality.

INTRODUCTION

Bone is a living mineralized material, highly complex and constantly remodeled in mass and architecture to adapt and repair the damage induced by growth, ageing and mechanical stress. In order to maintain a constant bone mass, bone remodeling necessitates a spatio-temporal coupling between osteoclasts, the bone-resorbing cells, and osteoblasts, the bone-forming cells. Bone remodeling is a complex process regulated by various stimuli that may affect osteoclast and osteoblast physiologies. A role for the gastro-intestinal tract in bone remodeling has been suggested with evidence that modulation of serum markers of bone resorption is mirrored with the profile of gut hormone release after a meal (Elnenaei, et al. 2010; Henriksen, et al. 2003).

Glucagon-like peptide-1 (GLP-1) is a gut hormone synthesized and secreted into the blood stream by intestinal endocrine L cells in response to a variety of stimuli (Wu, et al. 2010). Biologically active GLP-1 is secreted as a 7-37 or 7-36 amide peptide which is rapidly inactivated to GLP-1(9-36) by cleavage at the site of the second N-terminal alanine amino acid residue by the aminopeptidase, dipeptidyl peptidase IV (DPP-IV) (Drucker and Nauck 2006). GLP-1 action is tightly controlled by DPP-IV as more than 50% of GLP-1 is inactivated before it reaches the systemic circulation and the half-life of circulating GLP-1 is less that 2 min (Baggio and Drucker 2007). Nevertheless, GLP-1 binds to its receptor, the GLP-1R, widely expressed in pancreatic islets, kidney, lung, heart, stomach, intestine and the central nervous system and this interaction results in activation of intracellular signaling (Bullock, et al. 1996; Campos, et al. 1994).

Although uncertainty persist to clearly demonstrate expression of the GLP-1R in bone cells, administration of GLP-1 or its enzyme resistant analogue exendin-4 for three days in normal and diabetic rats results in increased trabecular bone mass and augmentation of the expression of osteoblast markers in these animals, suggesting a possible anabolic effect of GLP-1 on trabecular bone (Nuche-Berenguer, et al. 2009; Nuche-Berenguer, et al. 2010). Using a model of GLP-1 signaling deficiency, Yamada et al., reported that GLP-1R knockout mice exhibit a trend for lower trabecular bone mass in the proximal metaphysis of the tibia (Yamada, et al. 2008). These authors also reported reduction in cortical BMD as evidenced by an experimental CT-based densitometry. Taken together, all these data support an anabolic role of the GLP-1/GLP-1R pathway in bone. However, despite these observations, little is known about the impact of the GLP-1/GLP-1R on bone strength. Bone strength depends on bone and mineral quantity and also on structural and material properties of the bone matrix. Microarchitecture and material properties including degree of mineralization, mineral maturity and collagen properties are known factors that influence bone strength (Chappard, et al. 2011).

The aims of the present study were to investigate bone strength and bone quality in GLP-1R knockout male mice. Our results suggest that GLP-1R-deficient male mice present with significant alterations of the cortical morphology and material properties that undoubtedly resulted in reduced bone strength. These findings support a positive role for the GLP-1/GLP-1R pathway in controlling bone strength.

MATERIAL AND METHODS

Animals

Sixteen-week-old male mice presenting a deletion of the GLP-1R (kindly provided by Prof. DJ Drucker, Toronto, Canada) were used in this study. The background and generation of GLP-1R-deficient mice used in this study were derived from an in-house breeding colony originally described elsewhere (Hansotia, et al. 2004). Age-matched wild-type (WT) mice bred in-house with the same C57BL/6 genetic background were used as controls. A total of 8 deficient and 15 control mice were used in this study. Animals were maintained on a 12h:12h light-dark cycle in a temperature-controlled room (21.5 ± 1°C). Animals were individually caged and received food and water *ad libitum*. All experiments were conducted according to United Kingdom Office regulations (UK Animals Scientific Procedures Act 1986) and European Union laws. Animals were sacrificed by lethal inhalation of CO_2 and left and right femurs were collected, cleaned of soft tissue. Left femurs were stored in 70% ethanol at 4°C whilst right femurs were frozen in a saline-soaked gauze and stored at -20°C until use. Figure 1 describes the experimental design.

Bone mechanical testing

Three-point bending experiment were performed on the right femur. Before mechanical testing, femurs were thaw overnight and rehydrated in saline for 24hrs at room temperature as described elsewhere (Ammann, et al. 2007). Three-point bending strength was measured with a constant span length of 10 mm. The press head as well as the two support points were rounded to avoid shear load and cutting. Femurs were positioned horizontally with the anterior surface facing upwards, centered on the support and the pressing force was applied vertically to the midshaft of the bone. Each bone was tested with a loading speed of 2 $mm.min^{-1}$ until failure with a 90N load cell. The load-time curve obtained was converted into a load-displacement curve by the MTS testSuite TW software (MTS, Créteil, France). Ultimate load and ultimate displacement were respectively defined as the maximum load and maximum displacement recorded before break-down of the bone. Stiffness was calculated as the slope of the elastic deformation of the bone. The total absorbed energy was defined as the total area under the load-displacement curve and represents the total energy absorbed by the midshaft femur. The yield was defined as the load necessary to initiate the transformation from elastic to plastic deformation. The post-yield energy was defined as the area under the load-displacement curve from yield until failure and represents the energy absorbed by bone during plastic deformation. Material properties such as ultimate strength, ultimate strain, elastic modulus, yield strength, breaking strength and work to fracture have been calculated from mechanical parameters according to previously published equations (Ritchie, et al. 2008; Turner and Burr 1993).

Quantitative x-ray microradiograph imaging

Bone mineral content was determined using qXRI. Briefly, digital X-ray images of the left femur were recorded at a 12-µm pixel resolution using a Faxitron MX20 device (Edimex, Angers, France) operating at 26 kV and a 4X magnification. The region of interest was located 6 mm below the growth plate (mid-shaft of the femur) and represented a height of 2 mm. The relative mineral content of

calcified tissues was determined as reported by Bassett et al. (Bassett, et al. 2012) with the following modifications. Briefly, a 1.5-mm thick steel plate, a 1.5-mm pure aluminum wire and a 1.5-mm thick polyester plate were used on each microradiograph and served as standards. Before converting the 16-bit DICOM images into 8-bit tiff images, the histogram was stretched from the polyester (gray level 0) to the steel (gray level 255) standards using ImageJ 1.45s. Increasing gradations of mineralization density were represented in 16 equal intervals using the 16-colours lookup table in ImageJ 1.45s. The frequency of occurrence of an i grey level (Fi) was calculated as follows:

$$F_i = 100 \times \frac{Ni}{Nt}$$

Where Ni represents the number of pixels with the i grey level and Nt the total number of pixels. The frequency distribution as a function of grey level was plotted and the mean grey level (GL_{mean}) of each bone was deduced from this distribution using the following formula:

$$GLmean = \sum \frac{F_i \times GLi}{100}$$

where GLi represents the value of the i grey level.

X-ray microcomputed tomography (MicroCT)

MicroCT analysis was performed in the proximal left femur with a Skyscan 1172 microtomograph (Bruker MicroCT, Kontich, Belgium) equipped with an X-ray tube working at 69 kV/100 µA. The pixel size was fixed at 3.75 µm, the rotation step at 0.25° and exposure was done with a 0.5-mm aluminum filter. The region of interest (VOI) was located 6-mm below the growth plate. External bone diameter (B.Dm in mm), marrow diameter (Ma.Dm in mm), cortical thickness (Ct.Th in µm), and cross-sectional moment of inertia (CSMI in mm^4) were measured with a lab-based routine made with ImageJ 1.45s (NIH, Bethesda, MD) according to guidelines and nomenclature proposed by the American Society for Bone and Mineral Research (Bouxsein, et al. 2010). Three-D models represent a region of interest of 2 mm centered 6 mm below the growth plate.

Bone Mineral Density Distribution measured by backscattered electron imaging.

Quantitative backscattered electron imaging was employed to determine the bone mineral density distribution (BMDD) as previously reported (Gaudin-Audrain, et al. 2013; Roschger, et al. 1998). Rapidly after 3-point bending, lower portions of the right femur diaphysis were embedded undecalcified in methylmethacrylate at 4°C. Polymethylmethacrylate blocks were then polished to a 1-µm finish with diamond particles, carbon-coated and observed with a scanning electron microscope (EVO LS10, Carl Zeiss Ltd, Nanterre, France) equipped with a five quadrant semi-conductor backscattered electron detector. The microscope was operated at 20 keV with a probe current of 120 pA and a working distance of 8.5 mm. The backscattered signal was calibrated using pure carbon (Z=6, mean grey level = 25), pure aluminum (Z=13, mean grey level =225) and pure silicium (Z=14, mean grey level =253) standards (Micro-analysis Consultants Ltd, St Ives, UK). For these contrast/brightness settings, the BSE grey level histogram was converted into weight percentage of calcium. Eventual changes in brightness and contrast due to instrument instabilities were checked by monitoring the current probe and imaging the reference material (C, Al and Si) every 15 min. The

cortical bone area was imaged at a 200X nominal magnification, corresponding to a pixel size of 0.5 µm per pixel. The grey levels distribution of each image was analyzed with a lab-made routine using Image J. Three variables were obtained from the bone mineral density distribution: Ca_{peak} is the most frequently observed calcium concentration, Ca_{mean} is the average calcium concentration and Ca_{width} is the width of the histogram at half maximum of the peak.

Nanomechanical testing

Nanoindentation tests evaluated the mechanical properties of the bone matrix. As nanoindentation assesses volume of material at a length scale less than that of individual microstructural features in bone, this technique avoids confounding factors such as bone microarchitecture and porosity that affect tissue properties at larger length scales such as 3-point bending. Tests were performed on the same sample used for qBEI measurements after rapid polishing. Briefly, femurs were rehydrated overnight in saline prior to nanoindentation testing. Eight indents were positioned in cortical bone 6-mm below the growth plate with a NHT-TTX system (CSM, Peseux, Switzerland) equipped with a Berkowitch diamond probe. The indents were done up to a depth of 900 nm with a loading/unloading rate of 40mN/min. At maximum load, a holding period of 15 seconds was applied to avoid creeping of the bone material. Maximum load, indentation modulus, hardness and dissipated energy were determined according to Oliver and Pharr (Oliver and Pharr 1992).

Fourier Transformed InfraRed spectroscopy (FTIR)

After 3 point bending, upper portions of the femur diaphysis were embedded in pMMA at 4°C. Sections of 4µm thickness were cut dry on a heavy duty microtome equipped with tungsten carbide knives (Leica Polycut S) and sandwiched between BaF_2 optical windows. Spectral analysis were obtained on a Bruker Vertex 70 spectrometer (Bruker optics, Ettlingen, Germany) interfaced with a Bruker Hyperion 3000 infrared microscope equipped with a standard single element Mercury Cadmium Telluride (MCT) detector (750-4000cm^{-1}). Infrared spectra were recorded at a resolution of 4cm^{-1}, with an average of 32 scans in transmission mode. Background spectral images were collected under identical conditions from the same BaF_2 windows at the beginning and end of each experiment to ensure instrument stability. For FTIR analysis, 10 spectra were acquired approximately 6-mm below the growth plate on cortical bone, corresponding to the fracture zone observed by 3 point bending, and analyzed with the Opus Software (release 5.5, Bruker). The contribution of the embedding polymethylmethacrylate (pMMA) and water vapor were corrected for each spectrum prior to baseline correction. Then individual spectra have been subjected to curve fitting using a commercial available software package (Grams/AI 8.0, Thermofisher scientific, Villebon sur Yvette, France). Briefly, using the Levenberg-Maquardt algorithm every absorption band is characterized by its area. The second derivative spectrum was used to determine the number and the position of the bands constituting every spectral interval. All bands were positioned at maximal intensities with a Gaussian shape. Position, height, width at half intensity and area were obtained. Peaks corresponding to amide I and II (1350-1725 cm^{-1}) and v1v3 phosphate (900-1200cm^{-1}) were considered for further analysis. The evaluated IR spectral parameters were (1) mineral-to-matrix ratio which reflects the degree of

mineralization of the bone matrix, calculated from the ratio of integrated areas of the phosphate υ1, υ3 band at 900-1200 cm^{-1} to the amide I band at 1585-1725 cm^{-1} ; (2) mineral maturity, which reflects the ratio of apatic vs. nonapatic domains, calculated as the ratio of the relative intensity of subbands at 1020 and 1030cm^{-1} of the phosphate band (Paschalis, et al. 1996);(3) carbonate-to-phosphate ratio was expressed by the ratio of integrated areas of the υ2 CO_3^{2-} region (850-890cm-1) to the υ1, υ3 phosphate band (900-1200cm^{-1}) (Boskey, et al. 2005) and (4) collagen maturity, determined as the relative ratio of subbands located at 1660 cm^{-1} and 1690 cm^{-1} of the amide I peak. Although multiple theories exists about the significance of this ratio (pyridinium trivalent to dehydrodihydroxylysinonorleucine divalent collagen cross-links, modifications of secondary structure of collagen molecules), this ratio indicates the maturity of the collagen of the bone matrix (Farlay, et al. 2011; Paschalis, et al. 2001).

Gene expression

Bone marrow cells were isolated from the long bones of 16 weeks-old WT animals by flushing tibias and femurs with alpha-MEM as previously reported (Mieczkowska, et al. 2012). For osteoblast differentiation, bone marrow cells were plated into a 25 cm^2 culture flask until confluency (~3 days). For osteoclast culture, bone marrow cells were cultured for 24hrs into a 25 cm^2 flask in alpha-MEM supplemented with 10% fetal calf serum, 2 mM L-glutamine, 100 U/ml penicillin and 100 μg/ml streptomycin to allow stromal cells attachment. Non adherent cells were then collected and plated in 24 well-plate in alpha-MEM supplemented with 10% fetal calf serum, 2 mM L-glutamine, 100 U/ml penicillin, 100 μg/ml streptomycin, 25 ng/ml macrophage-colony stimulating factor (M-CSF-R&D systems, Abingdon, UK) and 50 ng/ml soluble RANKL (peprotech Ltd, London, UK). After seven days of culture, multinucleated osteoclasts were evidenced in culture as previously described (Mabilleau, et al. 2011). Total RNA were extracted from osteoblast or osteoclast ex vivo cultures, lung, pancreatic islets and heart using TriZol, reversed transcribed using iScript cDNA synthesis kit (Bio-Rad) and amplified by real-time PCR using SYBR GREEN PCR master mix (Bio-Rad). The mouse *Glp1r* mRNA transcript was amplified by quantitative PCR using primer pairs 5'-GGGTCTCTGGCTACATAAGGACAAC-3' and 5'-AAGGATGGCTGAAGCGATGAC-3'. The expression level of each sample was normalized against *gapdh* mRNA expression using primer pairs 5'-AATGGATTTGGACGCATTGGT-3' and 5'-TTTGCACTGGTACGTGTTGAT-3'.

Statistical analysis

Results were expressed as mean ± standard error of the mean (SEM). Non-parametric Mann-Whitney U-test was used to compare the differences between the groups using the Systat statistical software release 13.0 (Systat software Inc., San Jose, CA). Correlation between material properties and collagen cross-link ratio was assessed by a least squares linear regression analysis. Differences at $p<0.05$ were considered significant.

RESULTS

GLP-1R is required for optimum bone strength

Bone strength of the femur was assessed by three-point bending and the results are presented Table 1. In GLP-1R KO mice, mechanical parameters such as ultimate load, yield load, stiffness, total absorbed and post-yield energies were reduced significantly by 17 %, 21%, 25 %, 34% and 26% respectively as compared with WT animals. No differences in ultimate displacement were observed between these two groups of animals. Material properties such as work to fracture and yield strength were significantly reduced in GLP-1R-deficient mice by 20%, 20% and 7% respectively as compared with WT mice. No significant differences were observed for ultimate strength, breaking strength, ultimate strain and elastic modulus.

GLP-1R-deficiency results in altered femoral mineral density and cortical geometry

As represented Figure 2A, the bone mineral content seemed lower in GLP-1R KO animals and indeed, the frequency of occurrence of grey level, representing the bone mineral content, was switched toward the left in GLP-1R KO mice indicating a lower bone mineral content. Furthermore, the mean grey level was significantly reduced by 5.2% in GLP-1R KO mice as compared with WT controls ($p=0.021$). Histomorphometric analysis of cortical bone (Figure 2B) revealed that B.Dm was reduced significantly by 6% in GLP-1R KO animals as compared with WT controls ($p=0.034$) whilst Ma.Dm was unchanged ($p=0.289$). Consequently, Ct.Th and CSMI were lowered significantly by 13% and 25% respectively in deficient animals as compared with WT ($p=0.034$ and $p=0.031$ respectively).

Nanomechanical properties of the bone matrix are reduced in GLP-1R KO mice

As compared with WT animals, GLP-1R-deficient animals exhibited a significant 19% decrease in maximum load, as well as a significant reduction in bone matrix hardness (-19%) (Table 2). The indentation modulus was unchanged between the two groups of animals but the energy dissipated was significantly reduced by 15% in GLP-1R deficient mice.

Collagen maturation but not mineral maturation is altered in GLP-1R KO mice

The bone mineral density distribution in the bone matrix was investigated by qBEI in WT and GLP-1R KO mice (Table 3). Interestingly, no differences were observed between the two groups of animals in any of the studied parameters, indicating that the profile of mineralization of the bone matrix was similar in both cases. Similarly, the mineral-to-matrix ratio determined from FTIR measurements was not significantly different between WT and GLP-1R -/- animals (Figure 3A). The mineral maturity and carbonate content were unchanged in GLP-1R -/- animals as compared with WT ($p=0.221$ and $p=0.536$ respectively). On the other hand, the ratio of trivalent mature over divalent immature collagen crosslinks was significantly decreased by 15% in GLP-1R -/- mice as compared with WT ($p=0.007$, Figure 3D). As shown in Figure 4, a positive correlation ($R^2=0.62$, $p<0.004$) was found between dissipated energy assessed by nanoindentation and the 1660/1690 cm^{-1} ratio assessed by FTIR.

However, no significant correlations were found between maximum load or hardness with the 1660/1690 cm^{-1} ratio (R^2=0.33, p=0.067 and R^2=0.13, p=0.268, respectively).

GLP-1R is not expressed in bone cells

As expected, a strong expression of GLP-1R was found in lung and pancreatic islets and to a lower extent in heart (Figure 5). On the other hand, *Glp-1r* transcripts were not found in either osteoblasts or osteoclasts.

DISCUSSION

In the present study, we investigated bone strength in a mouse model of GLP-1R deficiency to understand how the GLP-1/GLP-1R pathway may affect bone strength. Three-point bending experiments, performed on the midshaft femur, revealed a significant decrease in the total absorbed energy as well as reduction in ultimate load, stiffness, yield load, post-yield energy, work to fracture and yield strength. These results suggest reduced bone strength in these animals. However, several factors might influence the outcome of three-point bending including bone microarchitecture and bone material properties (Turner and Burr 1993). Indeed, material properties calculated from stress-strain curves indicated that work to fracture and yield strength were significantly reduced in deficient animals but not ultimate strength or strain or the elastic modulus. Taken together these data indicate that cortical bone morphology and material properties may be altered. In the C57BL/6 mouse strain, at the midshaft femur, bone tissue is composed almost exclusively of cortical bone (Bouxsein, et al. 2005; Judex, et al. 2004). A study conducted by Yamada et al, reported a reduction in cortical BMD in the same GLP-1R -/- mice model in the tibia (Yamada et al. 2008). In the present study, cortical bone morphology was investigated by microCT and significant reductions in bone outer diameter, cortical thickness and cross-sectional moment of inertia were observed in GLP-1R -/- mice. Interestingly, cortical thickness diminution was associated with a decrease in the outer bone diameter whilst the marrow diameter was unchanged. Furthermore, gene expression analysis revealed that the GLP-1R is not expressed in bone cells suggesting that the decrease in bone strength and quality observed in this animal model may be a consequence of GLP-1R deletion in other tissues rather than a direct effect on bone cells.

Indeed, the GLP-1R is expressed in paraventricular, arcuate and dorsomedial nuclei of the hypothalamus (Merchenthaler, et al. 1999). Some of these regions have been implicated in the central control of bone remodeling by targeting osteoblasts and as such, alterations of bone quality could also result from activation/inactivation of specific central relays. Furthermore, these mice present with a mild glucose intolerance represented by fasting hyperglycemia (Ayala, et al. 2010). Regarding the beneficial role of insulin in bone growth and or quality, dysregulation of insulin action in these mice may also represent another mechanism leading to the observed phenotype. Furthermore, alterations of IGF-1R expression have been noted in these mice (Cornu, et al. 2009) and could also participate to the reduction in bone diameter and hence bone quality. The GLP-1R is also expressed in C cells of the thyroid gland and exerts, when activated by GLP-1 or its stable analogues, a stimulating effect on

calcitonin secretion in rodents (Bjerre Knudsen, et al. 2010). Calcitonin is one of the most efficient inhibitors of bone resorption in vitro (Moonga, et al. 1992; Zaidi, et al. 1990). Evidence from previous studies suggests that basally, male GLP-1R KO mice present with a 2.5 fold increase in circulating plasma calcitonin (Madsen, et al. 2012). As regard to the inhibitory action of calcitonin on bone resorption, it would be legitimate to hypothesize that bone resorption should be the primary target of calcitonin increase. However, recent evidence made with genetic ablation of either the calcitonin or calcitonin receptor genes highlighted an unexpected phenotype of high bone mass with no or little apparent effect on bone resorption (Dacquin, et al. 2004; Davey, et al. 2008; Hoff, et al. 2002). This unexpected phenotype indicated a possible inhibitory action (direct or indirect) of calcitonin on bone formation without affecting bone resorption. Therefore, the contributing effect of increased circulating calcitonin to bone formation in our GLP-1R KO model remains a possible scenario.

Another factor that strongly affects bone strength is the quality of the bone matrix (Ammann et al. 2007). GLP-1R KO mice presented with a decrease in maximum load (-17%), hardness (-19%) and dissipated energy (-15%). Owing to the nanocomposite composition of the bone matrix, any of the collagen or mineral might be involved in the reduction in material properties. Investigation of the bone mineral, by qBEI and FTIR, revealed that neither the degree of mineralization nor the maturity of the mineral was affected by the GLP-1R deletion. However, it is important to bear in mind that due to instrument limitations, we were not capable of investigating mineral cristallinity as proposed by Farlay et al (Farlay, et al. 2010). On the other hand, the maturity of the collagen matrix, determined as the 1660/1690 cm^{-1} ratio, was significantly reduced. Some controversies exist in the interpretation of this ratio as some groups reported that this ratio represent the trivalent over divalent cross-links ratio but recently an elegant study of Farlay and collaborators demonstrated that variation in this parameter could be more related to secondary structure of the collagen matrix after mineralization than a ratio of trivalent over divalent collagen crosslinks (Farlay et al. 2011). Nevertheless, it is an indicator of collagen maturity. The reduction of collagen maturity could itself explain the reduction in material properties, as we found a significant positive association between collagen maturity and dissipated energy. Furthermore, alteration of the collagen matrix often alters the post-yield properties of the bone matrix (Bailey, et al. 1999; Burr 2002; Zioupos, et al. 1999). In our study, the observed reduction in mature trivalent crosslinks could also account for the decreased post-yield energy determined by 3-point bending.

In conclusion, mice lacking the GLP-1R appear to have a decrease in bone strength observed at the anatomical level with a decrease in three-point bending resistance and decreased cortical thickness. Bone strength was also reduced at the tissue level and was associated with reductions of collagen crosslinking but no alteration of the bone mineral. Overall these data support a beneficial role for the GLP-1/GLP-1R signaling pathway in bone quality. This is important regarding the introduction of GLP-1 mimetics for the treatment of patients with type 2 diabetes mellitus.

DECLARATION OF INTEREST

The authors declared no conflict of interest that could be perceived as prejudicing the impartiality of the research reported.

FUNDING

This work was supported by grants from Contrat Région Pays de la Loire: Bioregos2 program and the University of Ulster Proof of Principle Funding Programme.

ACKNOWLEDGEMENTS

The authors are grateful to N. Gaborit and G. Brossard for their help with microCT. The authors would like also to acknowledge Mr Stéphane Blouin (Vienna, Austria) for fruitful discussion on FTIR methodology and measurements and Professor DJ Drucker (Toronto, Canada) for kindly providing the GLP-1R KO mice.

REFERENCES

Ammann P, Badoud I, Barraud S, Dayer R & Rizzoli R 2007 Strontium ranelate treatment improves trabecular and cortical intrinsic bone tissue quality, a determinant of bone strength. *J Bone Miner Res* **22** 1419-1425.

Ayala JE, Bracy DP, James FD, Burmeister MA, Wasserman DH & Drucker DJ 2010 Glucagon-like peptide-1 receptor knockout mice are protected from high-fat diet-induced insulin resistance. *Endocrinology* **151** 4678-4687.

Baggio LL & Drucker DJ 2007 Biology of incretins: GLP-1 and GIP. *Gastroenterology* **132** 2131-2157.

Bailey AJ, Sims TJ, Ebbesen EN, Mansell JP, Thomsen JS & Mosekilde L 1999 Age-related changes in the biochemical properties of human cancellous bone collagen: relationship to bone strength. *Calcif Tissue Int* **65** 203-210.

Bassett JH, van der Spek A, Gogakos A & Williams GR 2012 Quantitative X-ray imaging of rodent bone by Faxitron. *Methods Mol Biol* **816** 499-506.

Bjerre Knudsen L, Madsen LW, Andersen S, Almholt K, de Boer AS, Drucker DJ, Gotfredsen C, Egerod FL, Hegelund AC, Jacobsen H, et al. 2010 Glucagon-like Peptide-1 receptor agonists activate rodent thyroid C-cells causing calcitonin release and C-cell proliferation. *Endocrinology* **151** 1473-1486.

Boskey AL, DiCarlo E, Paschalis E, West P & Mendelsohn R 2005 Comparison of mineral quality and quantity in iliac crest biopsies from high- and low-turnover osteoporosis: an FT-IR microspectroscopic investigation. *Osteoporos Int* **16** 2031-2038.

Bouxsein ML, Boyd SK, Christiansen BA, Guldberg RE, Jepsen KJ & Muller R 2010 Guidelines for assessment of bone microstructure in rodents using micro-computed tomography. *J Bone Miner Res* **25** 1468-1486.

Bouxsein ML, Myers KS, Shultz KL, Donahue LR, Rosen CJ & Beamer WG 2005 Ovariectomy-induced bone loss varies among inbred strains of mice. *J Bone Miner Res* **20** 1085-1092.

Bullock BP, Heller RS & Habener JF 1996 Tissue distribution of messenger ribonucleic acid encoding the rat glucagon-like peptide-1 receptor. *Endocrinology* **137** 2968-2978.

Burr DB 2002 The contribution of the organic matrix to bone's material properties. *Bone* **31** 8-11.

Campos RV, Lee YC & Drucker DJ 1994 Divergent tissue-specific and developmental expression of receptors for glucagon and glucagon-like peptide-1 in the mouse. *Endocrinology* **134** 2156-2164.

Chappard D, Basle MF, Legrand E & Audran M 2011 New laboratory tools in the assessment of bone quality. *Osteoporos Int* **22** 2225-2240.

Cornu M, Yang JY, Jaccard E, Poussin C, Widmann C & Thorens B 2009 Glucagon-like peptide-1 protects beta-cells against apoptosis by increasing the activity of an IGF-2/IGF-1 receptor autocrine loop. *Diabetes* **58** 1816-1825.

Dacquin R, Davey RA, Laplace C, Levasseur R, Morris HA, Goldring SR, Gebre-Medhin S, Galson DL, Zajac JD & Karsenty G 2004 Amylin inhibits bone resorption while the calcitonin receptor controls bone formation in vivo. *J Cell Biol* **164** 509-514.

Davey RA, Turner AG, McManus JF, Chiu WS, Tjahyono F, Moore AJ, Atkins GJ, Anderson PH, Ma C, Glatt V, et al. 2008 Calcitonin receptor plays a physiological role to protect against hypercalcemia in mice. *J Bone Miner Res* **23** 1182-1193.

Drucker DJ & Nauck MA 2006 The incretin system: glucagon-like peptide-1 receptor agonists and dipeptidyl peptidase-4 inhibitors in type 2 diabetes. *Lancet* **368** 1696-1705.

Elnenaei MO, Musto R, Alaghband-Zadeh J, Moniz C & Le Roux CW 2010 Postprandial bone turnover is independent of calories above 250 kcal. *Ann Clin Biochem* **47** 318-320.

Farlay D, Duclos ME, Gineyts E, Bertholon C, Viguet-Carrin S, Nallala J, Sockalingum GD, Bertrand D, Roger T, Hartmann DJ, et al. 2011 The ratio 1660/1690 cm(-1) measured by infrared microspectroscopy is not specific of enzymatic collagen cross-links in bone tissue. *PLoS One* **6** e28736.

Farlay D, Panczer G, Rey C, Delmas PD & Boivin G 2010 Mineral maturity and crystallinity index are distinct characteristics of bone mineral. *J Bone Miner Metab* **28** 433-445.

Gaudin-Audrain C, Irwin N, Mansur S, Thorens B, Flatt PR, Basle MF, Chappard D & Mabilleau G 2013 Glucose-dependent insulinotropic polypeptide receptor deficiency leads to modifications of trabecular bone mass and quality in mice. *Bone* **53** 221-230.

Hansotia T, Baggio LL, Delmeire D, Hinke SA, Yamada Y, Tsukiyama K, Seino Y, Holst JJ, Schuit F & Drucker DJ 2004 Double incretin receptor knockout (DIRKO) mice reveal an essential role for the enteroinsular axis in transducing the glucoregulatory actions of DPP-IV inhibitors. *Diabetes* **53** 1326-1335.

Henriksen DB, Alexandersen P, Bjarnason NH, Vilsboll T, Hartmann B, Henriksen EE, Byrjalsen I, Krarup T, Holst JJ & Christiansen C 2003 Role of gastrointestinal hormones in postprandial reduction of bone resorption. *J Bone Miner Res* **18** 2180-2189.

Hoff AO, Catala-Lehnen P, Thomas PM, Priemel M, Rueger JM, Nasonkin I, Bradley A, Hughes MR, Ordonez N, Cote GJ, et al. 2002 Increased bone mass is an unexpected phenotype associated with deletion of the calcitonin gene. *J Clin Invest* **110** 1849-1857.

Judex S, Garman R, Squire M, Donahue LR & Rubin C 2004 Genetically based influences on the site-specific regulation of trabecular and cortical bone morphology. *J Bone Miner Res* **19** 600-606.

Mabilleau G, Chappard D & Sabokbar A 2011 Role of the A20-TRAF6 axis in lipopolysaccharide-mediated osteoclastogenesis. *J Biol Chem* **286** 3242-3249.

Madsen LW, Knauf JA, Gotfredsen C, Pilling A, Sjogren I, Andersen S, Andersen L, de Boer AS, Manova K, Barlas A, et al. 2012 GLP-1 receptor agonists and the thyroid: C-cell effects in mice are mediated via the GLP-1 receptor and not associated with RET activation. *Endocrinology* **153** 1538-1547.

Merchenthaler I, Lane M & Shughrue P 1999 Distribution of pre-pro-glucagon and glucagon-like peptide-1 receptor messenger RNAs in the rat central nervous system. *J Comp Neurol* **403** 261-280.

Mieczkowska A, Basle MF, Chappard D & Mabilleau G 2012 Thiazolidinediones induce osteocyte apoptosis by a G protein-coupled receptor 40-dependent mechanism. *J Biol Chem* **287** 23517-23526.

Moonga BS, Alam AS, Bevis PJ, Avaldi F, Soncini R, Huang CL & Zaidi M 1992 Regulation of cytosolic free calcium in isolated rat osteoclasts by calcitonin. *J Endocrinol* **132** 241-249.

437 Nuche-Berenguer B, Moreno P, Esbrit P, Dapia S, Caeiro JR, Cancelas J, Haro-Mora JJ & Villanueva-
438 Penacarrillo ML 2009 Effect of GLP-1 treatment on bone turnover in normal, type 2 diabetic, and
439 insulin-resistant states. *Calcif Tissue Int* **84** 453-461.
440 Nuche-Berenguer B, Moreno P, Portal-Nunez S, Dapia S, Esbrit P & Villanueva-Penacarrillo ML 2010
441 Exendin-4 exerts osteogenic actions in insulin-resistant and type 2 diabetic states. *Regul Pept* **159** 61-
442 66.
443 Oliver WC & Pharr GM 1992 An improved technique for determining hardness and elastic modulus
444 using load and displacement sensing indentation experiments. *J Mater Res* **7** 1564-1583.
445 Paschalis EP, DiCarlo E, Betts F, Sherman P, Mendelsohn R & Boskey AL 1996 FTIR
446 microspectroscopic analysis of human osteonal bone. *Calcif Tissue Int* **59** 480-487.
447 Paschalis EP, Verdelis K, Doty SB, Boskey AL, Mendelsohn R & Yamauchi M 2001 Spectroscopic
448 characterization of collagen cross-links in bone. *J Bone Miner Res* **16** 1821-1828.
449 Ritchie RO, Koester KJ, Ionova S, Yao W, Lane NE & Ager JW, 3rd 2008 Measurement of the
450 toughness of bone: a tutorial with special reference to small animal studies. *Bone* **43** 798-812.
451 Roschger P, Fratzl P, Eschberger J & Klaushofer K 1998 Validation of quantitative backscattered
452 electron imaging for the measurement of mineral density distribution in human bone biopsies. *Bone* **23**
453 319-326.
454 Turner CH & Burr DB 1993 Basic biomechanical measurements of bone: a tutorial. *Bone* **14** 595-608.
455 Wu T, Rayner CK, Jones K & Horowitz M 2010 Dietary effects on incretin hormone secretion. *Vitam*
456 *Horm* **84** 81-110.
457 Yamada C, Yamada Y, Tsukiyama K, Yamada K, Udagawa N, Takahashi N, Tanaka K, Drucker DJ,
458 Seino Y & Inagaki N 2008 The murine glucagon-like peptide-1 receptor is essential for control of bone
459 resorption. *Endocrinology* **149** 574-579.
460 Zaidi M, Datta HK, Moonga BS & MacIntyre I 1990 Evidence that the action of calcitonin on rat
461 osteoclasts is mediated by two G proteins acting via separate post-receptor pathways. *J Endocrinol*
462 **126** 473-481.
463 Zioupos P, Currey JD & Hamer AJ 1999 The role of collagen in the declining mechanical properties of
464 aging human cortical bone. *J Biomed Mater Res* **45** 108-116.

465

466

467

FIGURE LEGENDS

Figure 1: Schematic representation of the experimental design used in this study

Figure 2: Bone mineral content and cortical bone morphology is altered in GLP-1R KO animals. (A), bone mineral content as determined by quantitative X-ray microradiograph is reduced in GLP1-R KO animals (Black line and bar) as determined by a shift to the left of the frequency of occurrence of grey pixel and lower value of GLmean as compared with WT (grey line and bar). (B) 3-D models of WT and GLP-1R KO femurs and (C) histomorphometric analysis of cortical bone in WT and GLP-1R KO mice. *: $p<0.05$ *vs.* WT animals and **: $p<0.01$ *vs.* WT animals

Figure 3: FTIR assessment of bone matrix properties. (A) Mineral-to-matrix ratio, (B) mineral maturity, (C) carbonate content and (D) collagen maturity. *: $p<0.05$ vs. WT animals and **: $p<0.01$ *vs.* WT animals

Figure 4: Regression analysis between maximum load (A), hardness (B) and dissipated energy (C) and 1660/1690 cm^{-1} ratio. Open circles represent WT, close circles represent GLP-1R KO mice. **: $p<0.01$ *vs.* WT

Figure 5: Expression of *Glp1r* gene in mice. RT-PCR analysis was performed using RNA prepared from lung, pancreatic islets, heart and ex vivo culture of osteoblasts and osteoclasts from WT mice. Results were normalized relative to levels of *gapdh* mRNA transcripts in the same sample. Data are mean ± SEM, n=3.

TABLES

Table 1: Three-point bending parameters in WT and GLP-1R KO mice

	WT (n=12)	GLP-1R KO (n=8)	p value
Ultimate load (N)	14.47 ± 0.35	11.95 ± 0.27 *	0.034
Ultimate displacement (mm)	0.31 ± 0.006	0.30 ± 0.033	1.000
Stiffness ($N.mm^{-1}$)	42.68 ± 0.85	31.92 ± 5.45 *	0.05
Total absorbed energy (N.mm)	2.33 ± 0.09	1.54 ± 0.24 *	0.021
Yield load (N)	11.83 ± 0.45	9.37 ± 0.42 *	0.021
Post-yield energy (N.mm)	1.52 ± 0.05	1.12 ± 0.12 *	0.048
Ultimate strength (MPa)	84.2 ± 2.0	82.9 ± 2.0	0.513
Breaking strength (MPa)	80.9 ± 3.4	79.2 ± 7.3	0.783
Ultimate strain	0.013 ± 0.001	0.011 ± 0.002	0.714
Elastic modulus (GPa)	3.0 ± 0.2	3.0 ± 0.5	0.513
Work to fracture ($KJ.m^{-2}$)	0.211 ± 0.007	0.168 ± 0.017*	0.047
Yield strength (MPa)	69.3 ± 1.7	64.2 ± 0.5 *	0.05

*: p<0.05 vs. WT animals

Table 2: Nanomechanical properties of the bone matrix

	WT (n=12)	GLP-1R KO (n=8)	p value
Maximum load (mN)	11.9 ± 0.6	9.9 ± 0.4 *	0.037
Hardness (MPa)	627.8 ± 34.4	510.7 ± 28.9 *	0.028
Indentation modulus (GPa)	12.9 ± 0.6	12.1 ± 0.4	0.203
Dissipated energy (mN.nm)	3189.7 ± 176.7	2708.6 ± 130.9 *	0.028

*: p<0.05 vs. WT animals

Table 3: Bone mineral density distribution in WT and GLP-1R deficient mice

	WT (n=12)	GLP-1R KO (n=8)	p value
Ca_{peak} (%)	26.9 ± 0.7	26.8 ± 0.7	1.00
Ca_{mean} (%)	26.3 ± 0.6	26.3 ± 0.7	0.936
Ca_{width} (%)	2.7 ± 0.1	2.9 ± 0.2	0.337

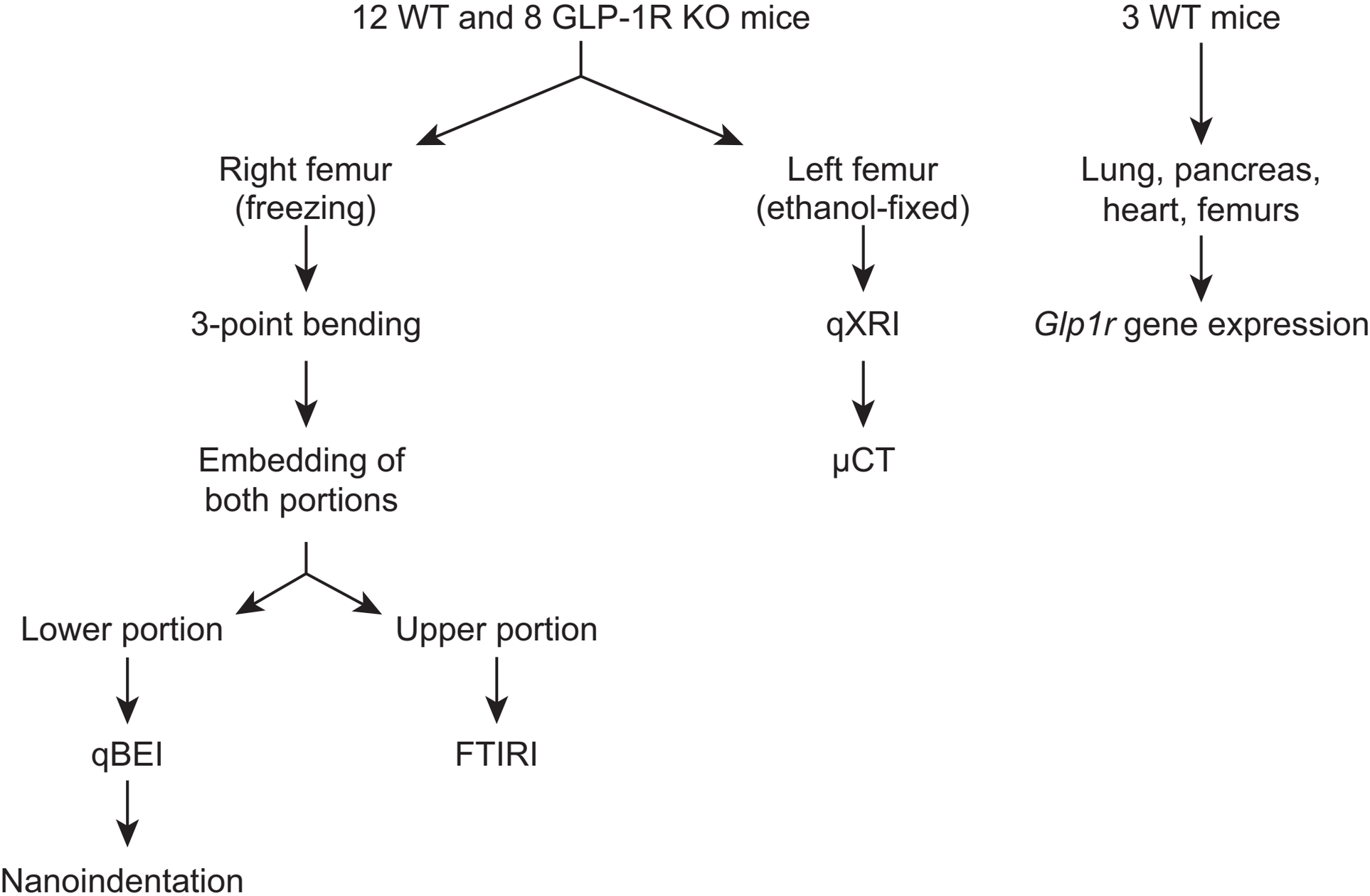
12 WT and 8 GLP-1R KO mice
3 WT mice
Right femur (freezing)
Left femur (ethanol-fixed)
Lung, pancreas, heart, femurs
3-point bending
qXRI
Glp1r gene expression
Embedding of both portions
µCT
Lower portion
Upper portion
qBEI
FTIRI
Nanoindentation

Figure 1

(A)

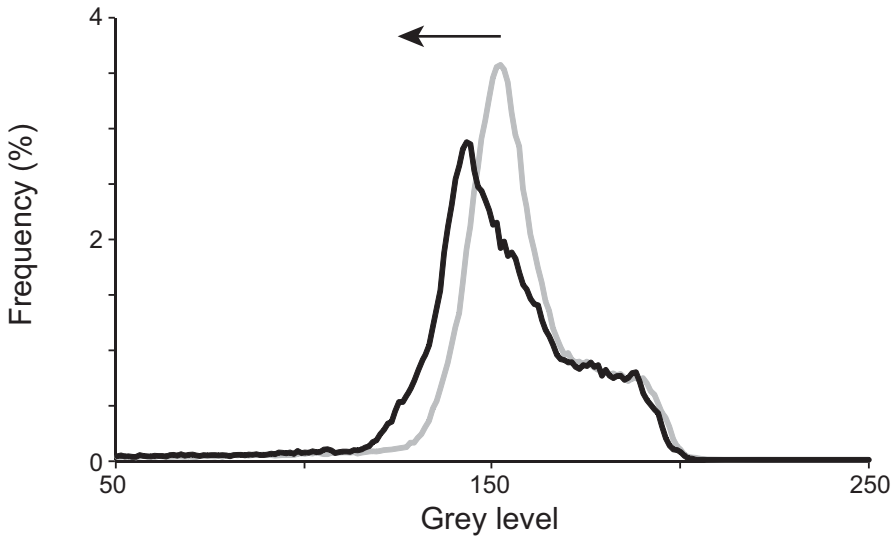
Frequency (%)
4
2
0
50
150
250
Grey level

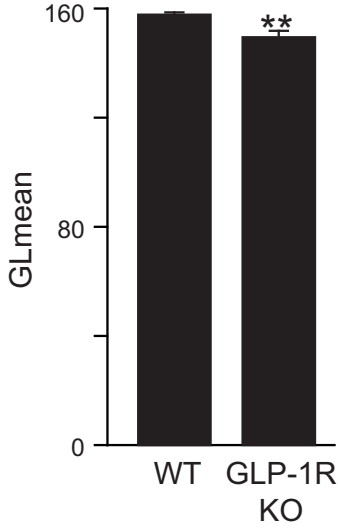
GLmean
160
80
0
**
WT
GLP-1R KO

(B)

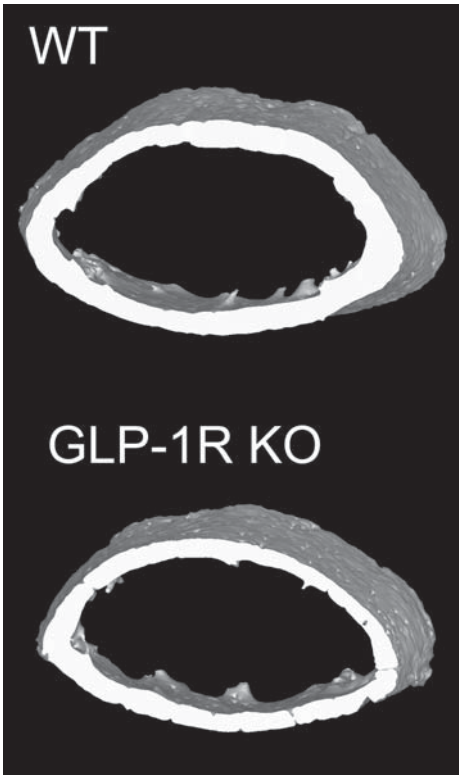
WT
GLP-1R KO

(C)

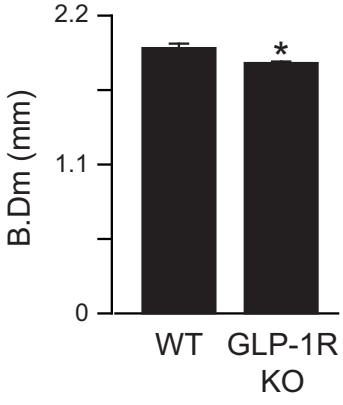
B.Dm (mm)
2.2
1.1
0
*
WT
GLP-1R KO

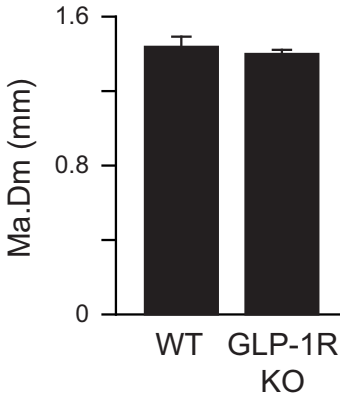
Ma.Dm (mm)
1.6
0.8
0
WT
GLP-1R KO

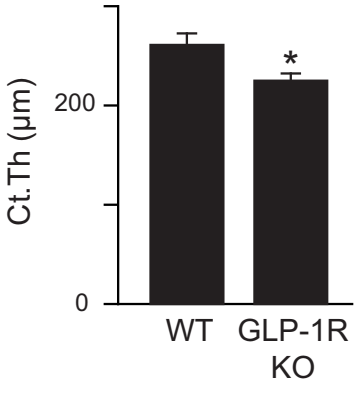
Ct.Th (µm)
200
0
*
WT
GLP-1R KO

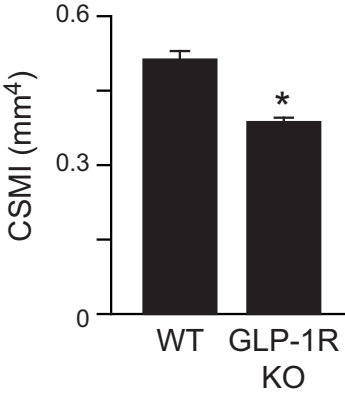
CSMI (mm4)
0.6
0.3
0
*
WT
GLP-1R KO

FIGURE 2

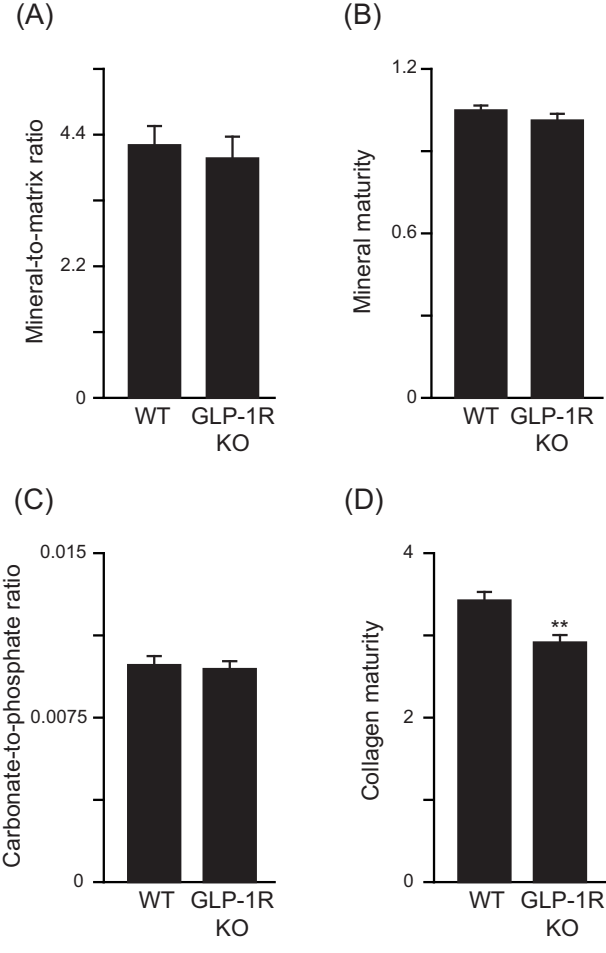
(A)
Mineral-to-matrix ratio
4.4
2.2
0
WT
GLP-1R KO
(B)
Mineral maturity
1.2
0.6
0
WT
GLP-1R KO
(C)
Carbonate-to-phosphate ratio
0.015
0.0075
0
WT
GLP-1R KO
(D)
Collagen maturity
4
2
0
**
WT
GLP-1R KO

FIGURE 3

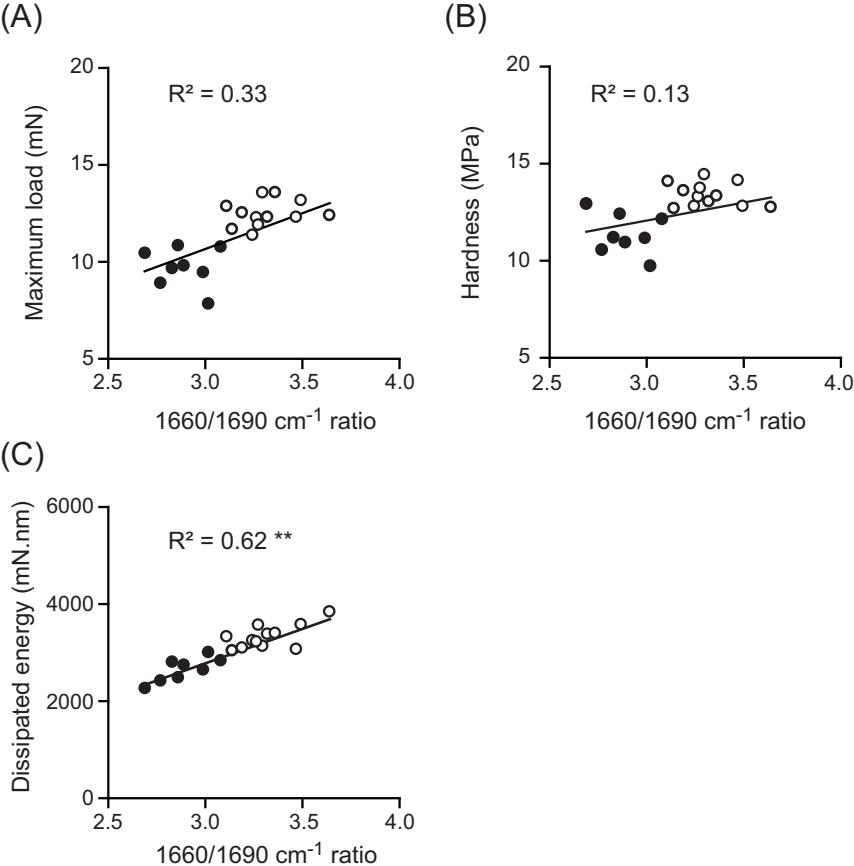
(A)
Maximum load (mN)
20
15
10
5
R² = 0.33
2.5
3.0
3.5
4.0
1660/1690 cm-1 ratio
(B)
Hardness (MPa)
20
15
10
5
R² = 0.13
2.5
3.0
3.5
4.0
1660/1690 cm-1 ratio
(C)
Dissipated energy (mN.nm)
6000
4000
2000
0
R² = 0.62 **
2.5
3.0
3.5
4.0
1660/1690 cm-1 ratio

FIGURE 4

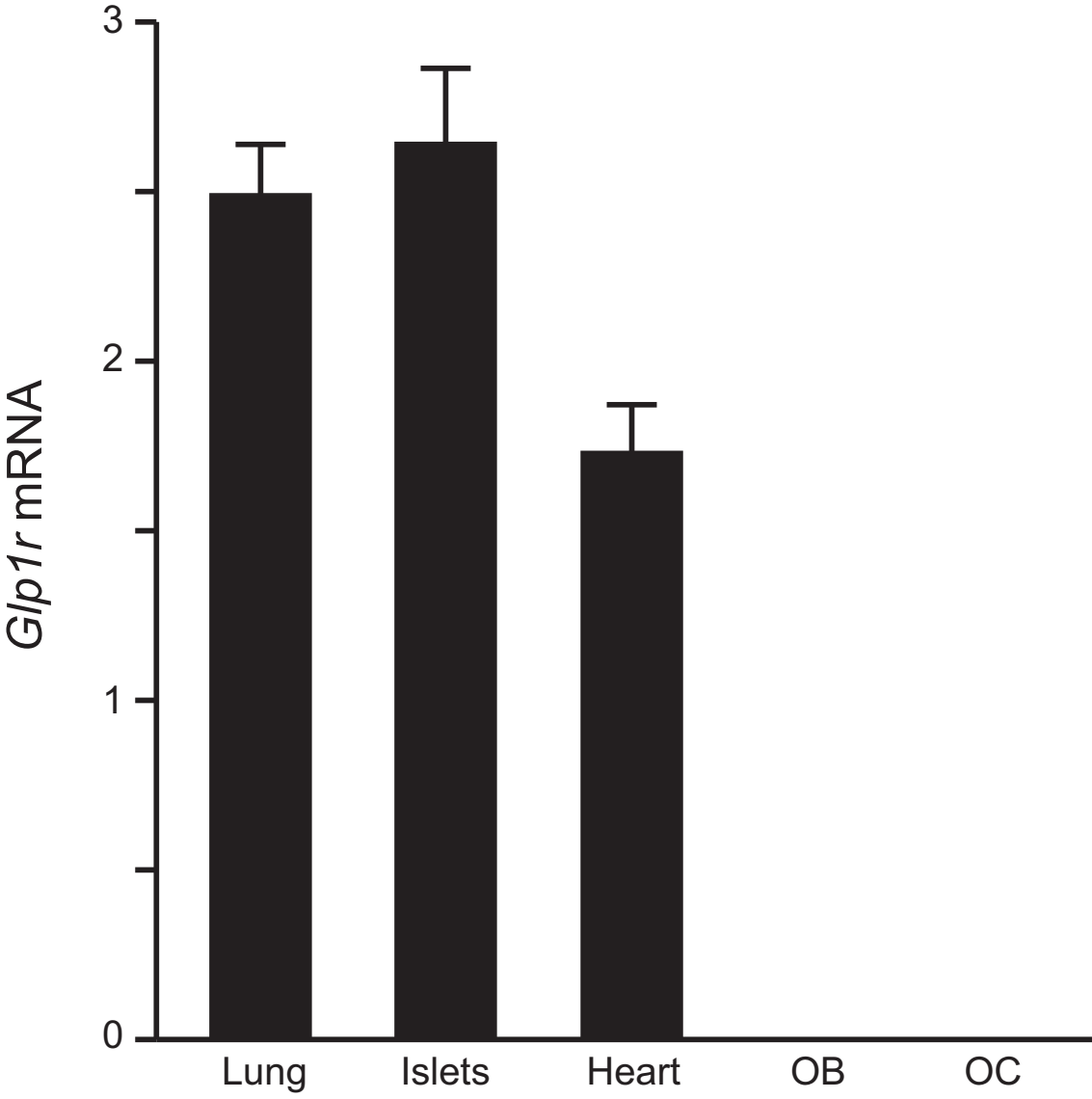

Figure 5